Research Article Vol. 30, No. 26 / 19 Dec 2022 / Optics Express 46861
Optics EXPRESS

Ultra-narrowband filter based on the metal-cladding resonant waveguide

HONG YANG,[1,4] HAILANG DAI,[1,4,5] AND XIANFENG CHEN[1,2,3,*]

[1]State Key Laboratory of Advanced Optical Communication Systems and Networks, School of Physics and Astronomy, Shanghai Jiao Tong University, Shanghai 200240, China
[2]Shanghai Research Center for Quantum Sciences, Shanghai 201315, China
[3]Collaborative Innovation Center of Light Manipulations and Applications, Shandong Normal University, Jinan 250358, China
[4]These authors contributed equally to this work
[5]hailangdai@sjtu.edu.cn
[*]xfchen@sjtu.edu.cn

Abstract: The simple and effective optical filter is the significantly scientific and technical interest in optical signal processing and communication. Especially, the development of microsystem integration is limited in traditional optical filters, due to the complicated structure, small choice, large cost, etc. In this paper, we report an ultra-narrowband filter based on a metal-cladding resonant waveguide. Therein, the ultra-narrowband resonant mode is achieved based on the resonance screening of incident light and cavity modes. According to the experimental data, the full width at half maximum (FWHM) can reach less than 0.1 nm. Furthermore, the resonant peak of FWMH is determined by the thickness of the waveguide, and the resonant wavelength can be selected by changing the incident angle.

1. Introduction

Narrow-band optical filter is one of the most important and common components in many fields, such as laser technology, optical modulation, optical communication, precision measurement, and optical sensing technology. The traditional narrow-band filters have their own characteristic. For example, the wavelength feature of the Fabry-Perot filter based on the principle of multi-beam interference [1–3] and Mach-Zehnder interferometer [4–7] is fixed once they are made. The low coupling efficiency of the incident light and mechanism of filters make it difficult for FWMH to reach 0.1 nm. The Fabry-Perot filter and Mach-Zehnder interferometer are also limited to polarization and high insertion loss. Meanwhile, the double-layer grating structure filter's single filter wavelength is closely related to the grating constant and the complex grating preparation, reducing the filter's usability and validity. Recently, the biofilm filtering technology [8] based on the interference effect of multilayer thin films, contributes to the high filter efficiency and broad applicability. However, the bandwidth is too large under the several layers. In order to achieve sub-nanometer bandwidth, it is necessary to prepare a hundred layers of thin films with strictly controlled thickness accuracy. Therein this technique is difficult to achieve and spend much time. Nowadays, the atomic resonance filter (ARF) with atomic resonance transition is used to novel filter of ultra-narrowband the signal light [9–12]. Its bandwidth can reach 0.001 nm and the intensity of output signal is amplified. However, the complex structure, low quantum conversion efficiency, and slow response time hold it back.

This letter reports an ultra-narrowband optical filter based on the double metal-cladding waveguide (DMCW). The ultrahigh-order modes (UOMs) in the waveguide layer of DMCW are excited according to the free-space coupling technology, when the incident light angle reaches the coupling angle [13]. Meanwhile, the UOMs is a series of wavelength-dependent attenuated total reflection (ATR) absorption peaks when the incident angle is fixed. Thus an optical comb can be

#475762 https://doi.org/10.1364/OE.475762
Journal © 2022 Received 15 Sep 2022; revised 27 Nov 2022; accepted 28 Nov 2022; published 8 Dec 2022

Optics EXPRESS

designed based on the resonance screening of incident light and cavity modes. Furthermore, the linewidth of ATR is less than 0.1 nm, and the wavelength of resonant is selected by changing the incident angle. This ultra-narrowband optical filter has simple sub-millimeter structure, convenient operation, and wide selectable range of resonance wavelength. It has potential applications in optical signal processing, spectral precision measurement, medical diagnosis, chemical analysis, and optical sensing.

2. Theory and simulation of structure

Figure 1(a) shows the structure of ultra-narrowband optical filter based on the DMCW. The waveguide structure of the filter is 10 mm long and 10 mm wide, including a 0.1-mm-thick BK7 glass slab as the base of the chip. The upper and lower surfaces of the glass slab are parallel (less than 2.8"). The glass slab is coated with metal films of different thicknesses on both sides. The incident light can be coupled into the DMCW by the upper silver film (about 29 nm thickness) due to the free electron resonance effect of metal. Another 300-nm-thick silver film is utilized as a substrate layer. In metal-cladding waveguide, the thin metal coupling layer and the small effective refractive index enable the direct coupling of light from the free space coupled into the guiding layer without any additional coupler, such as a grating or high-index prism [14–20]. When the incident angle of light is small, the standing optical field oscillates rapidly through the linear cavity between the metallic coupling layer and substrate [Fig. 1(b)], resulting in various properties of waveguide, such as strong field enhancement, high sensitivity, high quality factor, and polarization independence [21–27]. Meanwhile, thousands of guided modes are excited in the waveguide. Most guided modes are still quasi-continuous when the waveguide thickness is among sub-millimeters, and the series of modes has been called ATR peaks in reflected spectrum. Figure 1(b) shows a series of wavelength-dependent ATR absorption peaks accordingly by wavelength scanning when the incident angle is θ.

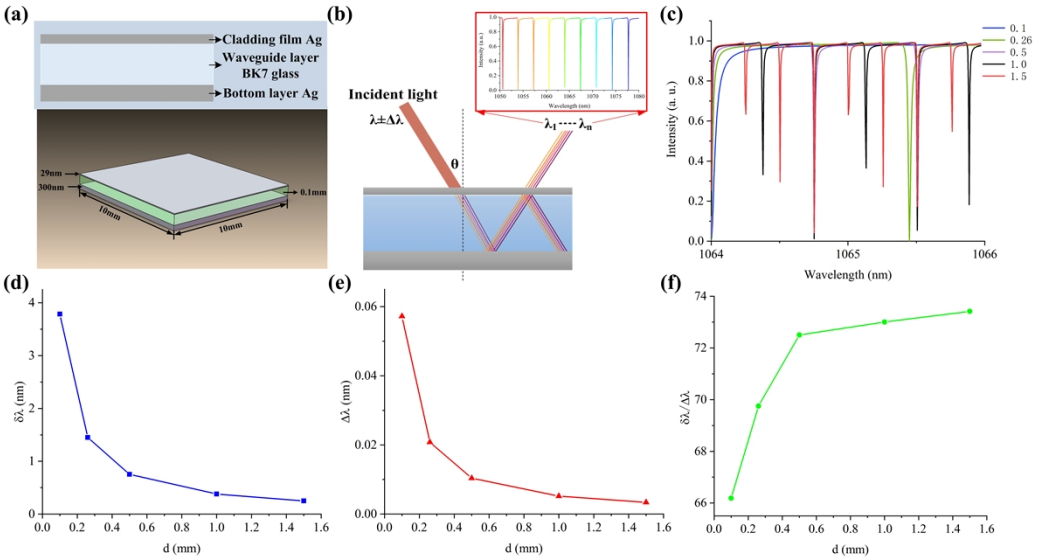

Fig. 1. Theory and simulation of the waveguide structure. (a) Schematic diagram of the waveguide structure. (b) Schematic diagram of the ATR peak spectrum of different wavelengths in the range of 1050-1080 nm wavelength incident light. (c) The ATR spectrum of different thickness of waveguide layer at the coupling angle. (d)-(f) The value of free space range, linewidth of mode, and duty cycle vary with thickness of the waveguide layer.

Optics EXPRESS

The Eq. (1) is the dispersion equation of the guided mode.

$$\kappa_1 d = m\pi + 2\arctan\left(\rho\frac{\alpha_2}{\kappa_1}\right) \tag{1}$$

where κ_1 is the x component of the wave vector k, $\kappa_1 = (k_0^2\varepsilon_1 - \beta^2)^{1/2}$, $\alpha_2 = (\beta^2 - k_0^2\varepsilon_2)^{1/2}$ and $k_0 = 2\pi/\lambda_0$ is the propagation constant in a vacuum. m is the number of modes. It can be expressed as

$$\kappa = k_0 n_1 \cos\theta \tag{2}$$

The parameters related to polarization are shown in the Eq. (3).

$$\rho = \begin{cases} 1 & TE \bmod e \\ \varepsilon_1/\varepsilon_2 & TM \bmod e \end{cases} \tag{3}$$

Since the mode number m > 1000, the polarization correlation Eq. (3) is ignored. The mode eigen equation can be approximately rewritten as the Eq. (4).

$$\frac{2\pi}{\lambda} n_1 d\cos\theta = m\pi \tag{4}$$

where d is the thickness of the guiding slab, θ is the incident angle of the light rays inside the waveguide. λ is the wavelength of the light in free space.

$$\frac{2\pi}{\lambda} = \frac{2\pi\nu}{c} \tag{5}$$

From the Eqs. (4) and (5), we can express the frequency spacing between two neighboring channels as the Eq. (6) without considering the material dispersion of the waveguide. $\Delta\nu$ is a constant when the incident angle of the light is fixed. In other words, the channel frequency spacings are equal for this comb filter.

$$\Delta\nu = \frac{c}{2n_1 d\cos\theta} \tag{6}$$

The Eq. (6) shows that the channel spacing can be tuned by changing the thickness of waveguide. The Eq. (4) shows the center wavelength can be tuned by changing the incident angle. This filter is insensitive to polarization but very sensitive to changes in wavelength and thickness of waveguide layer (see Supplement 1). We numerically simulated the ATR spectra of several waveguide layer with different thicknesses, as shown in Fig. 1(c). When the incident light is in the range of 1064-1066 nm, there are more ATR peaks in the 1.5-mm-thick waveguide. The number of ATR peaks increases with the thickness of the waveguide, as shown in Eq. (4). We calculated results of the ATR spectrum with the thickness of the waveguide layer by theory of waveguide in Fig. 1(c). Figures 1(d) and 1(e) present the wavelength spacing and linewidth of the ATR peaks, which decrease with increasing the thickness of waveguide layer. As shown in Fig. 1(f), the duty cycle increases with the thickness of waveguide.

According to the theory of DMCW, a continuous wave incident light with wavelength of 1064 nm is used to irradiate the waveguide after the collimating eyelet and attenuator. The optical signal is received by PD on the $\theta/2\theta$ synchronous rotator, as shown in Fig. 2(a). When incident angle reaches the coupling angle, the incident light is coupled into waveguide layer, and the UOMs are excited in the waveguide. Meanwhile, the number of m values of UOMs is proportional to the thickness of waveguide layer which means the density of modes changed. When the thickness of the waveguide layer reaches a millimeter-scale, the DMCW can accommodate thousands of

Optics EXPRESS

guided modes. For example, using the parameters: $\varepsilon_2 = -52.2 + i2.2$ (The metal material is Ag), $\varepsilon_1 = 2.278$, s = 29 nm (s is the thickness of the cladding film), d = 0.38 mm and $\lambda = 1064$ nm, m is 1657 for the highest mode. When the light beam is coupled from the free-space with a large incident angle, it is difficult to differentiate the adjacent guide modes because the mode density in the DMCW is extremely large and the corresponding ATR dips overlap with each other. On the other hand, a series of discrete guided modes can be excited at certain extremely small incident angles [10].

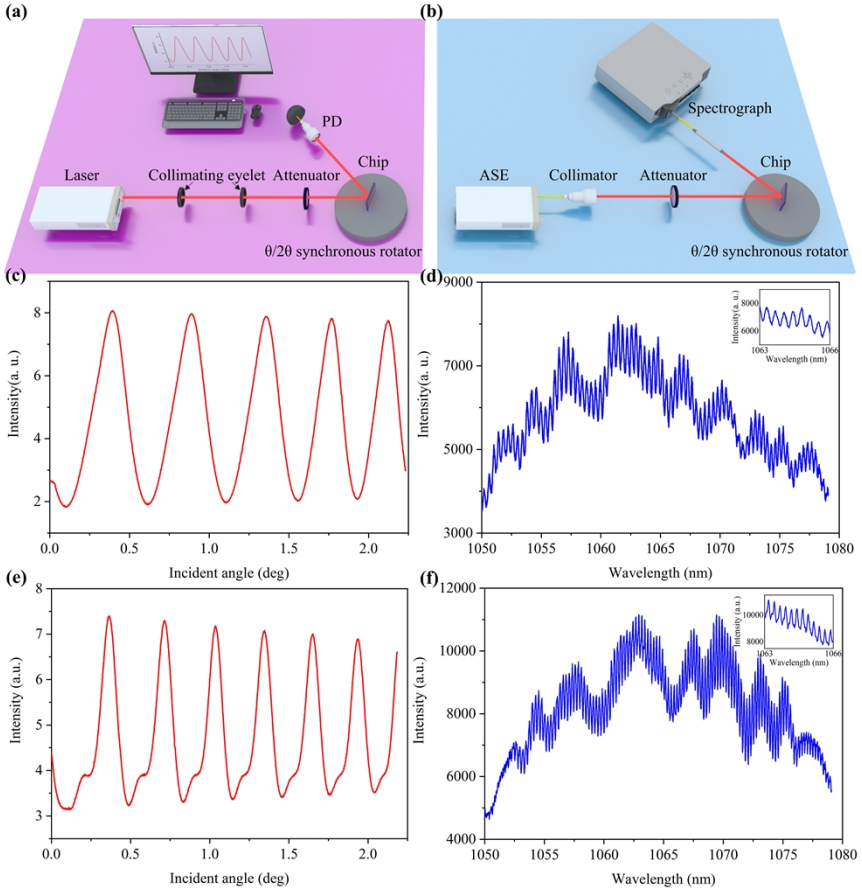

Fig. 2. Experimental schematics and results of the ultra-narrowband filter. (a) Experimental schematic for testing the reflectance spectra, the chip is fixed on the θ/2θ synchronous rotator and rotated by a personal computer (PC). (b) Experimental schematic and setup to obtain the analytical from spectrometer by scanning the incident wavelength. (c) Reflectance spectra of the 1.0-mm-thick waveguide versus the incident angle. (d), (f) The filter of the ASE source after passing through the 1.0 mm and 1.5 mm thickness of waveguides respectively. (e) Reflectance spectra of the 1.5-mm-thick waveguide versus the incident angle.

In our experiments, the thickness of glass slab is 1.0 mm and 1.5 mm respectively. The coupling efficiency of the incident light in the waveguide is high enough. Figures 2(c) and 2(e) show the reflection spectra of 1.0 mm and 1.5 mm thick waveguide (Au film) at coupling efficiencies of 76.5% and 57.5% respectively. Since the incident light is a broadband light source in the wavelength range of 1000-1100 nm, we selected the dielectric constants of Au when the incident light wavelength is 1000, 1064 and 1100 nm for comparison [28], and then calculated the corresponding theoretical number of guided modes (see Supplement 1). When the

Optics EXPRESS

incident light is 1000 nm, the dielectric constant of Au is $\varepsilon_1 = -38.968$, $\varepsilon_2 = 3.8500$, and the theoretical band 1000-1100 nm mode number m = 272. When the incident light is 1064 nm, the dielectric constant of Au is $\varepsilon_1 = -44.961$, $\varepsilon_2 = 4.3989$, and the theoretical band 1000-1100 nm mode number m = 272. When the incident light is 1100 nm, the dielectric constant of Au is $\varepsilon_1 = -48.496$, $\varepsilon_2 = 4.7104$, and m = 273. As can be seen, the incident light in the wavelength range of 1000-1100 nm has little effect on the guided mode number and filtering effect. We choose the dielectric constant of Au to be $\varepsilon_1 = -44.961$, $\varepsilon_2 = 4.3989$ (relative permittivity) in the theoretical calculation.

3. Experimental schematics

An amplified spontaneous emission (ASE) broadband light source with a wavelength range of 1000-1100 nm is irradiated on the surface of the DMCW at the coupling angle, and use a spectrometer (Zolix DR-05059, made in China) to analyze the reflected light in the range of 1050-1080 nm [Fig. 2(b)]. The comb filtering can be achieved, as shown in Figs. 2(d) and 2(f), therein the fluctuation of the spectrum shape is due to the power difference at each wavelength. Meanwhile, each ATR peak does not separate into separate identifiable peaks due to 0.1 nm the maximum resolution of the spectrometer. ASE light source is knocked on the chip surface at a coupling angle after a collimator and an attenuator. Figures 2(d) and 2(f) are the reflected light spectrum of the thickness of waveguide layer (an optical chip) of 1.0 and 1.5 mm respectively. The corresponding filtered linewidth changes from 0.16 to 0.10 nm when the thickness of the waveguide increases from 1.0 to 1.5 mm.

4. Results and discussion

According to the experimental data of the 1.0 mm and 1.5 mm thickness of waveguide layer, the ATR peak of the FWHM is less than 0.10 nm. The selectivity of the filter is simply achieved by slight rotation of the sample with respect to the incident light beam. Differing from the chip coupling system, the free space coupling technology offers a maximum angular range which can be varied from the normal to graze direction with respect to the waveguide plane. According to the dispersion Eq. (1) of the DMCW and $n_{eff} = n_0 \sin\theta_0$, we can obtain an approximate relationship between two peak wavelengths of the filter at the normal reflection ($\theta_0 = 0°$, λ_0) and the graze reflection ($\theta_0 = 90°$, λ). Resulting in $\frac{\lambda_0}{\lambda} = \sqrt{\frac{\varepsilon_1}{\varepsilon_1 - \varepsilon_0}}$. The ratio of the maximal peak length to the minimal peak length is 1.34 in case of $\varepsilon_1 = 2.25$ and $\varepsilon_0 = 1.0$. It indicates that the tuning range can be larger than 100 nm. Therefore, we verify and compare the filtering characteristics of several different thicknesses (0.1–1.5 mm) of waveguides layer with the highest coupling efficiency (see Supplement 1) and compare with the theoretical simulation of Fig. 1(c). The $\delta\lambda/\Delta\lambda$ in Table 1 is the duty cycle calculated according to the theoretical simulation of Fig. 1(c). We found that as the thickness of the waveguide is thicker, the distance between the peak is smaller, the linewidth is about smaller accordingly (the minimum can reach 0.10 nm), and the duty cycle is more significant, as shown in Table 1. These trends are consistent with the theoretical simulation of Fig. 1(c).

In order to observe the filtering effect of the DMCW, the FWHM 3.9 nm broad-band filter and 1.17 nm narrow-band filter (TIR filter) based on the interference effect of multilayer thin films, which contributes to the high filter efficiency and broad applicability, has been utilized in the experimental system respectively, as shown in Fig. 3. The broad-band and narrow-band filter spectra are described in Supplement 1. When the broad-band filter is added into system and the chip thickness is 1.0 mm, we can obtain more than 20 peaks on the linewidth of 3.9 nm transmission spectrum, as shown in Fig. 3(a). Meanwhile, there are three peaks on the linewidth of 1.17 nm transmission spectrum when the narrow-band filter has been utilized in system [Fig. 3(b)]. It means that the 0.16 nm line-band light beam is achieved. At the same conditions,

Optics EXPRESS

Table 1. Filtering Characteristics of Waveguides with Different Thicknesses

	Theory			Experiment	
Thickness(mm)	$\delta\lambda(nm)$	$\Delta\lambda(nm)$	$\delta\lambda/\Delta\lambda$	$\delta\lambda(nm)$	$\Delta\lambda(nm)$
0.1	3.79	0.06	66.18	2.80	1.10
0.26	1.45	0.02	69.75	1.51	0.76
0.5	0.75	0.01	72.50	0.68	0.40
1.0	0.38	0.01	73.00	0.38	0.16
1.5	0.25	0.01	73.42	0.22	0.10

1.5-mm-thick of chip finally filter out 0.10 nm line-band light beam, as shown in Figs. 3(c) and 3(d). $\Delta\lambda_1 - \Delta\lambda_4$ are the actual linewidth measured by the spectrometer, $\Delta\lambda_5$ and $\Delta\lambda_6$ are the linewidth of the narrow band peak estimated from the duty cycle of the spectrum. The specific calculation method can be derived by referring to the formula of Supplement 1. Details of the filtering effect after broad-band filter or narrow-band filter for other thickness waveguides are given by Supplement 1.

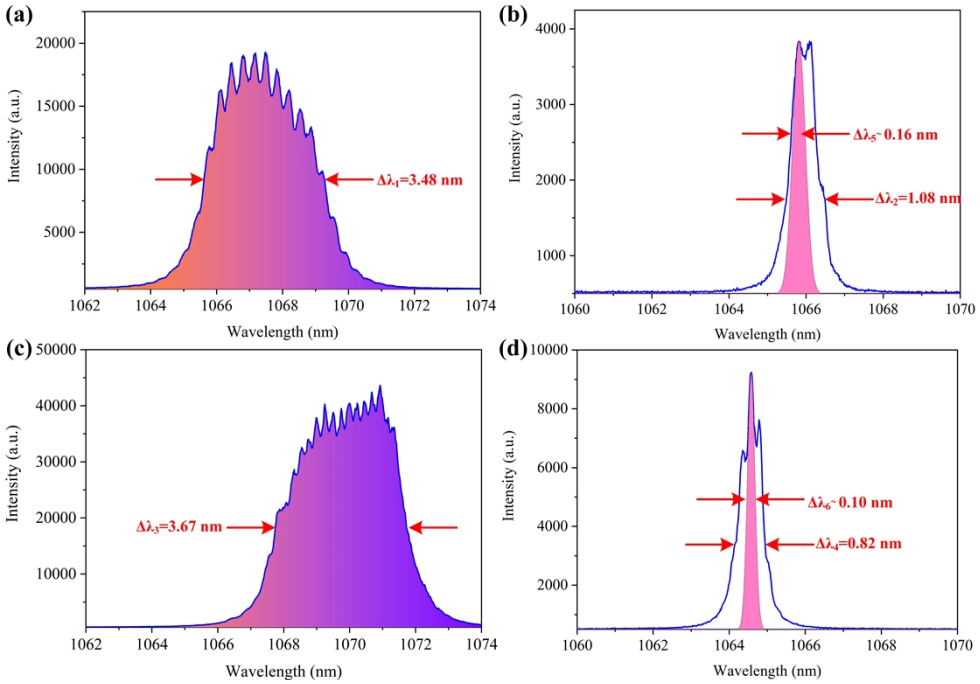

Fig. 3. Filtering effect after adding broad-band filter and narrow-band filter to the optical path respectively. (a), (b) The effect of the 1.0-mm-thick waveguide filtering with broad-band filter and narrow-band filter. (c), (d) The effect of the 1.5-mm-thick waveguide filtering with broad-band filter and narrow-band filter.

According to the theory of waveguide, the wavelength of coupled and output light are related to the incident light. With the same experimental conditions, we choose the wavelength of the output light by modulating the incident angle. As shown in Fig. 4, the comb filtering 1064-1074 nm is achieved through a 1.5 mm thick waveguide. A broadband filter with a linewidth of 3.9 nm is utilized to the optical path, the experimental data as shown in Fig. 4(a). When changing the incident angle of the chip as shown in Figs. 4(b)–4(e), we can obtain a narrow-band output light

Optics EXPRESS

with a central wavelength of 1064.55-1065.49 nm. The tuning range can reach more than 15% of the incident light wavelength.

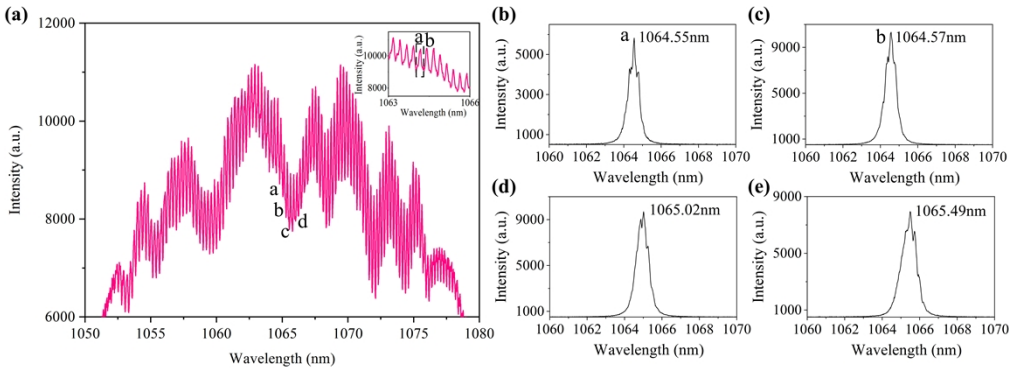

Fig. 4. The comb filtering come true from 1064 nm to 1074 nm with a 1.5-mm-thick waveguide. (a) The filter of the ASE source after passing through the waveguide about 1.5 mm thick. (b)-(e) Adjusting the incident angle of the waveguide to filter out different wavelengths of light.

Due to the maximum resolution of the spectrometer in experiment (0.1 nm), we are difficult to resolve the two adjacent ATR peaks from more than 1.0-mm-thick waveguide. In order to prove the selectable property of chip, we continue to tune the optical signal for 0.1 and 0.26 mm thick waveguides by changing the incident angle of the ASE light source (The corresponding specific incidence angles have been marked in Fig. 5). The linewidth is 1.10 nm for the waveguide layer

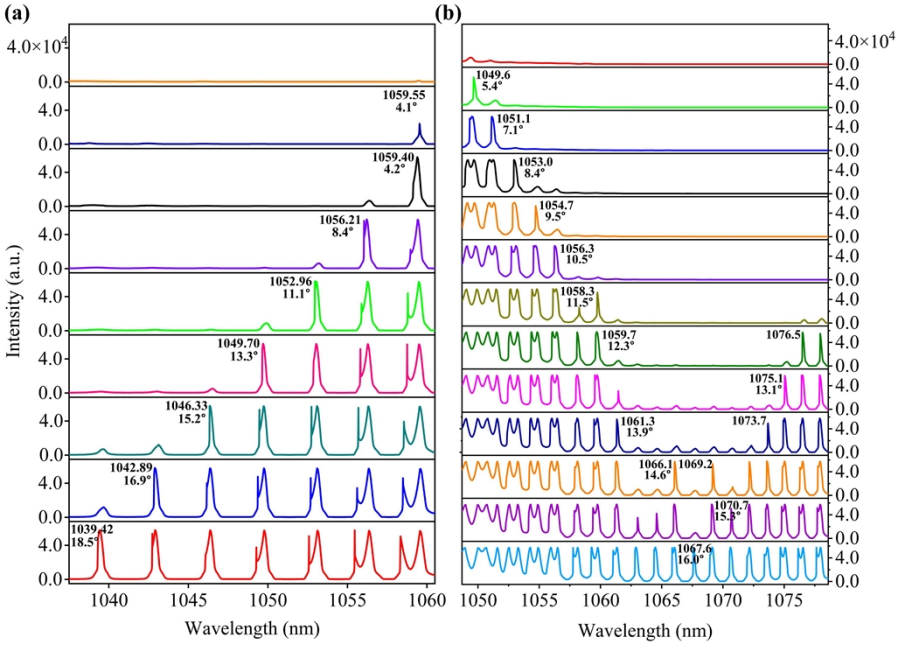

Fig. 5. The number of filter peaks varies with the incident angle. (a) The effect of the 0.1-mm-thick waveguide filtering. (b) The effect of the 0.26-mm-thick waveguide filtering. The abscissa is the wavelength range of the optical signal received by the spectrometer.

Optics EXPRESS

thicknesses of 0.1 mm, and the other linewidth is 0.76 nm for the waveguide layer thicknesses of 0.26 mm. We found that the wavelength of peaks after filtering varies with the incident angle of light. Meanwhile, the number of peaks is different for 0.1 and 0.26 mm thick waveguides. Eventually, multiple discrete narrow-band peaks will appear.

5. Conclusion

We propose a new method for an ultra-narrowband optical filter. The optical filter is based on a double metal-cladding waveguide without a complex structure or specifical materials. It uses free-space coupling technology to achieve dynamic regulation of filtered lasers with different linewidths by changing the thickness of the waveguide. The device not only has the characteristics of the sizeable dynamic tuning range, narrow filter bandwidth, high transmittance, high sensitivity, and quality factor, but also has the advantages of simple structure, convenient control, easy fabrication and low cost. This new type of ultra-narrowband filter has broad application prospects in photonic integrated chips, chemical analysis, biosensing, medical diagnosis and other fields.

Funding. National Key Research and Development Program of China (2017YFA0303701, 2018YFA0306301); National Natural Science Foundation of China (11734011, 11764020, 11974245, 12104298); Shanghai Municipal Science and Technology Major Project (2019SHZDZX01-ZX06).

Disclosures. The authors declare no conflicts of interest.

Data availability. Data underlying the results presented in this paper are not publicly available at this time but may be obtained from the authors upon reasonable request.

Supplemental document. See Supplement 1 for supporting content.

References

1. C. Williams, N. Hong, M. Julian, S. Borg, and H. J. Kim, "Tunable mid-wave infrared Fabry-Perot bandpass filters using phase-change GeSbTe," Opt. Express **28**(7), 10583–10594 (2020).
2. X. Q. Wu, Q. S. Chen, Y. P. Wang, X. T. Tan, and X. D. Fan, "Stable High-Q Bouncing Ball Modes inside a Fabry–Pérot Cavity," ACS Photonics **6**(10), 2470–2478 (2019).
3. A. Bourgade and J. Lumeau, "Large aperture, highly uniform narrow bandpass Fabry–Perot filter using photosensitive As_2S_3 thin films," Opt. Lett. **44**(2), 351–354 (2019).
4. G. Zhou, R. Kumar, Q. Wu, W. P. Ng, R. Binns, N. Lalam, X. Miao, L. Niu, X. Yuan, Y. Semenova, G. Farrell, J. Yuan, C. Yu, X. Sang, X. Xin, B. Liu, H. Lv, and Y. Q. Fu, "A simple all-fiber comb filter based on the combined effect of multimode interference and Mach-Zehnder interferometer," Sci. Rep. **8**(1), 11803–8 (2018).
5. H. N. Xu, D. X. Dai, and Y. C. Shi, "Low-crosstalk and fabrication-tolerant four-channel CWDM filter based on dispersion-engineered Mach-Zehnder interferometers," Opt. Express **29**(13), 20617–20631 (2021).
6. F. Horst, W. M. Green, S. Assefa, S. M. Shank, Y. A. Vlasov, and B. J. Offrein, "Cascaded Mach-Zehnder wavelength filters in silicon photonics for low loss and flat pass-band WDM (de-)multiplexing," Opt. Express **21**(10), 11652–11658 (2013).
7. Q. Z. Deng, L. Liu, R. Zhang, X. B. Li, J. Michel, and Z. P. Zhou, "Athermal and flat-topped silicon Mach-Zehnder filters," Opt. Express **24**(26), 29577–29582 (2016).
8. T. Erdogan and V. Mizrahi, "Thin-film filters come of age," *Photonics Spectra* 37, 94–96 (2003).
9. W. Zhang, L. Stern, D. Carlson, D. Bopp, Z. Newman, S. Kang, J. Kitching, and S. B. Papp, "Ultranarrow Linewidth Photonic-Atomic Laser," Laser Photonics Rev. **14**(4), 1900293 (2020).
10. L. F. Yin, B. Luo, J. Y. Xiong, and H. Guo, "Tunable rubidium excited state Voigt atomic optical filter," Opt. Express **24**(6), 6088–6093 (2016).
11. S. Q. Liu, Y. D. Zhang, H. Wu, and P. Yuan, "Ultra-narrow bandwidth atomic filter based on optical-pumping-induced dichroism realized by selectively saturated absorption," Opt. Commun. **285**(6), 1181–1184 (2012).
12. Y. F. Wang, X. G. Zhang, D. Y. Wang, Z. M. Tao, W. Zhuang, and J. B. Chen, "Cs Faraday optical filter with a single transmission peak resonant with the atomic transition at 455 nm," Opt. Express **20**(23), 25817–25825 (2012).
13. Q. H. Wei, H. L. Dai, H. R. Shan, H. G. Li, Z. Q. Cao, and X. F. Chen, "All-photonic synapse based on iron-doped lithium niobate double metal-cladding waveguides," Phys. Rev. B **104**(23), 235308 (2021).
14. H. G. Li, Z. Q. Cao, F. Lu H, and Q. S. Shen, "Free-space coupling of a light beam into a symmetrical metal-cladding optical waveguide," Appl. Phys. Lett. **83**(14), 2757–2759 (2003).
15. H. L. Dai, B. Jiang, C. Yin, Z. Q. Cao, and X. F. Chen, "Ultralow-threshold continuous-wave lasing assisted by a metallic optofluidic cavity exploiting continuous pump," Opt. Lett. **43**(4), 847 (2018).
16. H. R. Shan, Q. H. Wei, H. L. Dai, and X. F. Chen, "Sensitive detection of orthogonal polarization intensity ratio via double metal-cladding waveguide," Opt. Laser Eng. **151**, 106920 (2022).

Optics EXPRESS

17. G. A. Wurtz, R. Pollard, W. Hendren, G. P. Wiederrecht, D. J. Gosztola, V. A. Podolskiy, and A. V. Zayats, "Designed ultrafast optical nonlinearity in a plasmonic nanorod metamaterial enhanced by nonlocality," Nat. Nanotechnol. **6**(2), 107–111 (2011).
18. H. F. Lu, Z. Q. Cao, H. G. Li, and Q. S. Shen, "Study of ultrahigh-order modes in a symmetrical metal–cladding optical waveguide," Appl. Phys. Lett. **85**(20), 4579–4581 (2004).
19. L. Chen, Z. Q. Cao, F. Ou, H. G. Li, Q. S. Shen, and H. C. Qiao, "Observation of large positive and negative lateral shifts of a reflected beam from symmetrical metal-cladding waveguides," Opt. Lett. **32**(11), 1432 (2007).
20. Y. L. Zheng, W. Yuan, X. F. Chen, and Z. Q. Cao, "Wideband slow-light modes for time delay of ultrashort pulses in symmetrical metal-cladding optical waveguide," Opt. Express **20**(9), 9409–9414 (2012).
21. H. L. Dai, C. Yin, Z. Y. Xiao, Z. Q. Cao, and X. F. Chen, "White Beam Lasing from a Hybrid Microcavity with SlabCapillary Mode Coupling," Phys. Rev. Appl. **11**(6), 064055 (2019).
22. H. L. Dai, C. Yin, X. N. Ye, B. Jiang, M. W. Ran, Z. Q. Cao, and X. F. Chen, "A possible pathogenetic factor of sicklecell disease based on fluorescent analysis via an optofluidic resonator," Sci. Rep. **7**(1), 3174 (2017).
23. S. E. Savotchenko, "Nonlinear surface waves propagating along composite waveguide consisting of nonlinear defocusing media separated by interfaces with nonlinear response," J. Nonlinear Optic. Phys. Mat. **29**(01n02), 2050002 (2020).
24. K. T. Kim, H. W. Kwon, J. W. Song, S. Lee, W. G. Jung, and S. W. Kang, "Polarizing properties of optical coupler composed of single mode side-polished fiber and multimode metal-clad planar waveguide," Opt. Commun. **180**(1-3), 37–42 (2000).
25. Y. Wang, Z. Q. Cao, T. Y. Yu, H. G. Li, and Q. S. Shen, "Enhancement of the superprism effect based on the strong dispersion effect of ultrahigh-order modes," Opt. Lett. **33**(11), 1276 (2008).
26. Q. Kang, D. Y. Shen, J. Sun, X. Luo, W. Liu, Z. H. Zhou, Y. Zhang, and W. J. Wan, "Optical brake induced by laser shock waves," J. Nonlinear Optic. Phys. Mat. **29**(03n04), 2050010 (2020).
27. D. Kumar and V. Singh, "Theoretical modeling of a nonlinear asymmetric metal-clad planar waveguide based sensors," Optik **122**(20), 1872–1875 (2011).
28. https://refractiveindex.info/?shelf=main&book=Au&page=Ciesielski.